Participation of a Cyanobacterial S Layer in Fine-Grain Mineral Formation

SUSANNE SCHULTZE-LAM,[1] GEORGE HARAUZ,[2] AND TERRY J. BEVERIDGE[1]*

Department of Microbiology[1] and Department of Molecular Biology and Genetics,[2] University of Guelph, Guelph, Ontario, Canada N1G 2W1

Cyanobacteria belonging to the *Synechococcus* group are ubiquitous inhabitants of diverse marine and freshwater environments. Through interactions with the soluble constituents of their aqueous habitats, they inevitably affect the chemistry of the waters they inhabit. *Synechococcus* strain GL24 was isolated from Fayetteville Green Lake, New York, where it has a demonstrated role in the formation of calcitic minerals. In order to understand the detailed interactions which lead to mineral formation by this organism, we have undertaken detailed ultrastructural studies of its cell surface and the initial events in mineral growth using a variety of electron microscopic and computer image enhancement techniques. *Synechococcus* strain GL24 has a hexagonally symmetrical S layer as its outermost cell surface component. The constituent protein(s) of this structure appears as a double band by sodium dodecyl sulfate-polyacrylamide gel electrophoresis with M_rs of 104,000 and 109,000. We demonstrate that the S layer acts as a template for fine-grain gypsum and calcite formation by providing discrete, regularly arranged nucleation sites for the critical initial events in the mineralization process. To our knowledge, this is the first time that a bacterial S layer has been shown to have a role in mineral formation in a natural environment, and this report provides conclusive evidence for the specific involvement of bacterial surfaces in natural mineral formation processes.

Synechococcus strain GL24 is a small, unicellular cyanobacterium that was isolated from Fayetteville Green Lake, New York. This lake is supplied by subsurface groundwater, which leads to density stratification and the maintenance of a permanent chemocline. It is relatively isolated from other water systems and has carbonate bioherms (modern, active stromatolites or thrombolites) growing outward from sunlit portions of the shoreline (22). The origin of these bioherms was a subject of great controversy for many years, until detailed work undertaken by Thompson and coworkers (22) showed that the structures were forming as a result of the activities of small, unicellular cyanobacteria belonging to the *Synechococcus* group. These cyanobacteria are the dominant phytoplankton present in the lake, and they are present in overwhelming abundance in the calcitic ($CaCO_3$) bioherm fabric itself. Subsequently, Thompson and Ferris (21) showed that the presence of these cells is a prerequisite for calcite formation because of their photosynthesis and the resulting alkalization of the microenvironment surrounding each cell. Although the natural pH (pH $\approx$7.9) of the lake water promotes gypsum ($CaSO_4 \cdot 2H_2O$) precipitation from abundant dissolved Ca^{2+} and SO_4^{2-}, this alkalization by the cells pushes the solid mineral field toward the formation of stable calcite crystals. Without photosynthesis and active alkalization, the pH around each cell remains at 7.9 and gypsum crystals are initiated and grow on the *Synechococcus* cell surface. The biomineralization of gypsum seems to be a two-step process initiated by the binding of calcium to the cell surface followed by the binding of sulfate to the calcium. In photosynthesizing cells, the sulfate is thought to eventually be replaced by carbonate to form calcite at the cell surface as the pH increases (21). Thus, the cells provide essential nucleation sites and the chemical conditions necessary for mineral formation. The actual site on the cell surface to which the calcium is bound has not previously been determined, but, intuitively, it should take place on some extracellular polymer produced by the cells.

Our preliminary ultrastructural studies have revealed that a hexagonally symmetrical, paracrystalline surface array (or S layer) resides above the typically gram-negative envelope of the Green Lake isolate (19). S layers are proteinaceous structures found surrounding the cells of diverse groups of both eubacteria and archaeobacteria. In many cases, detailed chemical and ultrastructural studies have been undertaken; these have been summarized in a recent review by Messner and Sleytr (15). Such layers were observed on cyanobacteria more than 20 years ago (10), but there have been few detailed investigations since then (11, 13). Because of the peripheral position of these S layers, their presence in a wide range of taxonomic groups, and the recognition that a considerable amount of energy must be expended by the organism for their synthesis, it is apparent that these layers must play a significant role in the life of the organism. Despite this fact, there seems to be no common function ascribable to S layers. The following proposed functions are varied, and they seem to reflect the diversity of the bacteria possessing them: protective layers, molecular sieves, molecule and ion traps, promoters of cell adhesion, agents of surface recognition, and the determinants of cell shape (15). In most investigations, however, the particular function of the S layer was not apparent.

The peripheral location of the *Synechococcus* S layer allows it to have intimate contact with soluble components of the external chemical environment. Because of the extensive mineralization associated with this cyanobacterium in the lake and in laboratory simulations (21, 22), it is important for us to gain a detailed knowledge of this S layer's physicochemistry. In the present study, we describe the detailed ultrastructure of the *Synechococcus* strain GL24 S layer and propose a novel function for this structure: that it serves as a template for fine-grain mineral formation.

---

* Corresponding author.

MATERIALS AND METHODS

Culture and growth conditions. *Synechococcus* strain GL24 was isolated from lake water by picking single colonies from agar plates of Cg10 medium (5) and suspending them in 1 ml of liquid medium. Freedom from contamination by heterotrophic organisms was assessed by direct microscopic examination and by streaking onto five different media (nutrient agar, *Pseudomonas* P medium, brain heart infusion agar, tryptic soy agar, and Cg10; all except the last from Difco) which were used at three different concentrations: full, 1/10, and 1/100 strength. Axenic cultures were used to inoculate 10 ml of Cg10. The cultures were subsequently scaled up to 100-ml volumes. Batch cultures of *Synechococcus* strains were grown as 100-ml volumes in 250-ml flasks under Grolux fluorescent lights with intensities of 20 microeinsteins $m^{-2} \cdot s^{-1}$. Cells were sensitive to higher light intensities. Cultures were grown for 4 weeks, until they reached stationary phase, and then used for our investigations.

Thin sections for electron microscopy. Cells from 2 ml of culture were pooled by centrifugation in microcentrifuge tubes and fixed in 4% (vol/vol) glutaraldehyde (Marivac) in 0.01 M HEPES (*N*-2-hydroxyethylpiperazine-*N'*-2-ethanesulfonic acid) (Research Organics) buffer, pH 7.2, for 24 h at 20°C in the dark. After being washed three times with buffer, the cells were postfixed in 2% (wt/vol) aqueous osmium tetroxide (Fisher) for 2 h at 20°C, washed, and treated with 2% (wt/vol) uranyl acetate (Fisher) for 1 h. The cells were washed three times with ultrapure water and suspended in molten 2% (wt/vol) Noble agar with a Pasteur pipette. Agar cores (extruded from the pipette) were cut into 5-mm lengths and placed in 7-ml borosilicate glass vials. The samples were dehydrated in a graded series of ethanol solutions, with each step lasting for 15 min. They were then immersed in ethanol-acetone (50:50) and 100% acetone for 10 min in each solution. Infiltration of samples by Epon 812 took place overnight in a mixture of 50% acetone–50% resin. The agar cores were then embedded in resin and allowed to polymerize at 60°C for 48 h. Thin sections were cut on a Reichert Ultracut E ultramicrotome with a diamond knife and collected on 200-mesh, Formvar- and carbon-coated copper grids. The sections were stained with 2% (wt/vol) uranyl acetate and 2% (wt/vol) lead citrate for 30 min with each stain prior to being viewed in the electron microscope.

Freeze-substitution. The protocol of Graham and Beveridge (6) was followed. Briefly, cell pellets were suspended in 18% (vol/vol) glycerol (as a cryoprotectant) in 0.01 M HEPES, pH 7.2, and incubated at 20°C for 20 min. The cells were then mixed 1:1 with 2% Noble agar and deposited as a thin smear on cellulose-ester filter supports. Small wedges were cut and quickly plunge-frozen in liquid propane held at liquid-nitrogen temperature. The wedges were then deposited in vials containing a substitution medium consisting of 2% (wt/vol) uranyl acetate–2% (wt/vol) osmium tetroxide in acetone. Substitution was allowed to occur at −70°C for 48 h. The samples were then removed and embedded in Epon 812 as described above.

Freeze fracture and -etching. Cells were suspended in 18% glycerol (as a cryoprotectant) for 15 min at 20°C, placed on gold planchets, and then plunge-frozen in liquid propane held at liquid-nitrogen temperature. Fracturing and etching were accomplished with the use of a Balzers BA 360M unit equipped with electron guns and a quartz monitor. Samples were etched for 30 s, shadowed with platinum, and coated with carbon, and replicas were prepared by hydrolyzing the bacteria with concentrated sulfuric acid and commercial bleach (Javex). The replicas were then picked up on clean, uncoated, 400-mesh copper grids for viewing with the electron microscope.

S-layer preparation for electron microscopy and electrophoresis. One-milliliter volumes of cell culture were removed and centrifuged at 12,000 × *g* in an Eppendorf microcentrifuge. The pellet was resuspended in 100 μl of ultrapure water and incubated at 60°C for 1 h. This induced shedding of the outer membrane material, with its attached S layer, which provided clean array fragments.

SDS-PAGE. Supernatants from S-layer preparations were mixed 1:1 with sample buffer containing 10% (wt/vol) sodium dodecyl sulfate (SDS)–5% (vol/vol) β-mercaptoethanol, boiled for 5 min, and subjected to discontinuous polyacrylamide gel electrophoresis (PAGE) using the buffer system of Laemmli (12). Gels were stained with one of the following stains: (i) Coomassie blue R250 to locate the S-layer protein, (ii) the silver stain of Morrisey (16) to indicate the presence of proteins, and (iii) the silver stain used by Hitchcock and Brown (9) to indicate the presence of lipopolysaccharide.

Negative staining for electron microscopy. Drops of prepared sample containing S-layer fragments were placed on small sheets of Parafilm and allowed to adsorb to 200-mesh, Formvar- and carbon-coated copper grids for 2 min. Excess sample was removed by blotting on filter paper, and the grid was transferred to a drop of 0.1% (wt/vol) peptone (as a wetting agent) for 10 s and then to 2% (wt/vol) aqueous uranyl acetate for 20 s. The grid was blotted dry between steps.

Electron microscopy. Specimens were viewed in a Philips EM300 transmission electron microscope at an accelerating voltage of 60 keV and operating under standard conditions with a liquid-nitrogen cold trap in place at all times.

Mineralization studies. Mineralization took place in filter-sterilized lake water and in a simulated lake water medium (GL medium), which was devised by using the values of major ion concentrations in the water of Fayetteville Green Lake reported by Brunskill and Ludlam (4). Duplicate flasks of lake water and GL medium were supplemented with additional nitrate (8 mM $NaNO_3$) and iron [2 μM $Fe_2(SO_4)_3$] to enhance the growth of the organism. The growth of *Synechococcus* strain GL24 and the accompanying mineral formation were monitored for 1 month. To learn whether calcium was specifically required for initiation of mineral formation by the S layer, GL medium was prepared with Ca, Mg, Ba, or Sr as the only major divalent cation added, with a reliance on the presence of trace amounts of Mg and Ca in the other reagents to support growth of the cells. The major divalent cations were added at concentrations of 0.5, 1, and 10 mM. The natural level of calcium in lake water is approximately 10 mM, but a range of concentrations was used because of the unknown toxicity levels of the other ions (especially Ba and Sr). For Ba and Sr, precipitates occurred in the medium during preparation, but enough remained in the solution after filtering to interact with the bacteria. At weekly intervals after inoculation, samples were removed, viewed, and micrographed as unstained whole mounts with the electron microscope. These electron microscope negatives were used for computer image processing.

EDS. Grids were viewed with a Philips EM400T transmission electron microscope equipped with a model LZ-5 light element detector and an exL multichannel analyzer (both from LINK Analytical) operating at 100 keV, with a cold trap in place, to obtain elemental analysis of the minerals. Energy-dispersive X-ray spectroscopy (EDS) spectra were

taken by using a beam current of 0.1 μA and a spot size of 400 nm. The typical counting time was 100 s (live time).

Electron image analysis. Selected S-layer patches were digitized with a Hitachi KP-113 solid-state television camera mounted on a dissecting microscope (Wild Leitz M3B) and interfaced to a Vision8 frame grabber (Everex) in an IBM-compatible personal computer. The digitized images were represented by arrays of picture elements (pixels), each corresponding to an area of 0.61 by 0.61 nm at the object level.

Analyses of digitized images were performed in the framework of the IMAGIC image-processing system (23). Since the S-layer patches were small, image enhancement by Fourier filtering was not as appropriate as direct correlation averaging (17). Areas of S-layer patches containing single, well-preserved morphological unit cells (hexamers) were extracted from the original image. The single-hexamer images were pretreated by band-pass filtering to suppress the very low and very high spatial frequencies. The very high spatial frequencies represented mostly noise, while the very low spatial frequencies represented unwanted information, e.g., gradual fluctuations in the average densities that depended largely on the amount and uniformity of specimen staining (7, 8). After band-pass filtering to enhance only the important structural information, the hexamers in each image were surrounded by a circular mask to cut away unnecessary background. The images were then standardized by floating within this mask to an average density of zero and by multiplication of each pixel by a factor to normalize the variance.

A computerized double-alignment algorithm based on cross-correlation functions was used to bring all of the morphological units into rotational and translational register with one another (7, 8). Those images with the highest correlation coefficients with respect to the final reference were then averaged together. This new average image represented the two-dimensional construction of a particular projection of the morphological unit of the S layer.

RESULTS

Thin sections and freeze-etching. In thin sections of conventionally prepared or freeze-substituted cells, the S layer appeared as a periodic peripheral layer that completely surrounded the cell (Fig. 1). Depending on how individual patches of an S layer were oriented to the plane of the cut, different patterns were revealed. When a cut was made parallel to a line of symmetry, the pattern showed up as a row of diamonds with a center-to-center spacing of 22 nm (Fig. 2). The centers of the diamonds were unstained, and this may be due to the fact that they are hollow or they contain a central mass of apolar residues that do not bind heavy-metal stains efficiently. Cuts that were perpendicular to the plane of symmetry revealed a row of parallel lines which may correspond to a side view of the diamonds (Fig. 3). Tangential cuts tended to show dots arranged in hexagonal patterns (Fig. 4). Thin sections of freeze-substituted cells gave similar patterns, but, in addition, they showed "stems" connecting the S layer to the underlying outer membrane (Fig. 5).

Freeze fractured and -etched specimens (Fig. 6) revealed that each encompassing S layer around a cell was a composite of smaller patches which met at lattice discontinuities rather than a nearly perfect crystal that completely surrounded the cell. This was also reflected in the thin sections (several orientations of S-layer particles were seen on each

cell) and, possibly, in the preparations used for negative staining (small S-layer pieces rather than large sheets tended to come off during 60°C treatment, and these could represent the individual elements of the patchwork mosaic which compose the S layer).

Negatively stained and mineralized S-layer patterns. Whole mounts of heat-treated cells negatively stained with uranyl acetate showed that the S layer tended to come off in fragments, often associated with outer membrane material, and revealed a delicate pattern that exhibited hexagonal symmetry (Fig. 7). Since many array fragments were also found without underlying outer membrane material, it was apparent that the outer membrane is not essential for the stability of the S-layer pattern. On more detailed examination (Fig. 8), it was apparent that this pattern was made up of a series of "pinwheels" composed of rings that were centers of sixfold symmetry joined by Y linkers whose centers were foci of threefold symmetry. The rings were 22 nm apart, and the distance from a ring center to the center of a Y linker was 11 nm.

When cells were grown in lake water or in GL medium with and without iron and nitrate supplements to enhance growth, gypsum ($CaSO_4 \cdot 2H_2O$) formation was initiated, and its development continued throughout the initial period of the 1-month study. This mineral was gradually replaced by calcite as time progressed and as pH increased. In unstained whole mounts, in which the only contrast came from the minerals present, the S-layer pattern was clearly seen in the early stages of mineralization and was always outlined in gypsum (Fig. 9). This was most commonly seen after 2 weeks of growth, when cells were present in sufficiently high numbers to provide a good sampling set but mineralization had not progressed to a point at which the cells were so encrusted as to obscure the pattern. Progressive stages of mineralization were easily discernible as the S-layer pattern was filled in and eventually became obscured by the growing gypsum crystals (Fig. 10 to 13). The identity of the mineral outlining the S-layer pattern was confirmed by EDS (Fig. 14).

Cells that were grown in the presence of Mg, Ba, and Sr did not show the S-layer pattern in unstained whole mounts, although there were mineral grains present on the cell surfaces. In the magnesium-grown samples, the cells appeared generally darkened, but there were no discrete sites of mineral formation, and it seemed that this cation did not provide suitable nucleation sites for mineral formation, as with calcium. It is noteworthy that the cells did grow in the presence of relatively high concentrations of barium and strontium and grew very well in magnesium, so the failure to form other minerals was not due to a lack of active, photosynthesizing cells. A limiting factor for the Ba and Sr samples was that these cations had a natural tendency to precipitate as sulfates at the pH used in this study (pH 7.9). This limited the effective concentration of soluble sulfate and Ba (or Sr) in the medium. Despite this fact, EDS showed that there was still sufficient Ba or Sr present in the fluid phase to participate in mineral formation on the cells.

Computer-enhanced imaging. When images similar to those in Fig. 8 were subjected to computer enhancement (Fig. 15), the S-layer structure was resolved to 2 to 3 nm (7). The primary morphological unit (made up of six subunits) appeared to be a pinwheel with arms describing a spiral. Two separate pore systems (i.e., regions of high stain density), those in the middle of the rings and those between the Y linkers, could be seen. The latter are large, diamond-shaped pores, making the array an open, lacy structure.
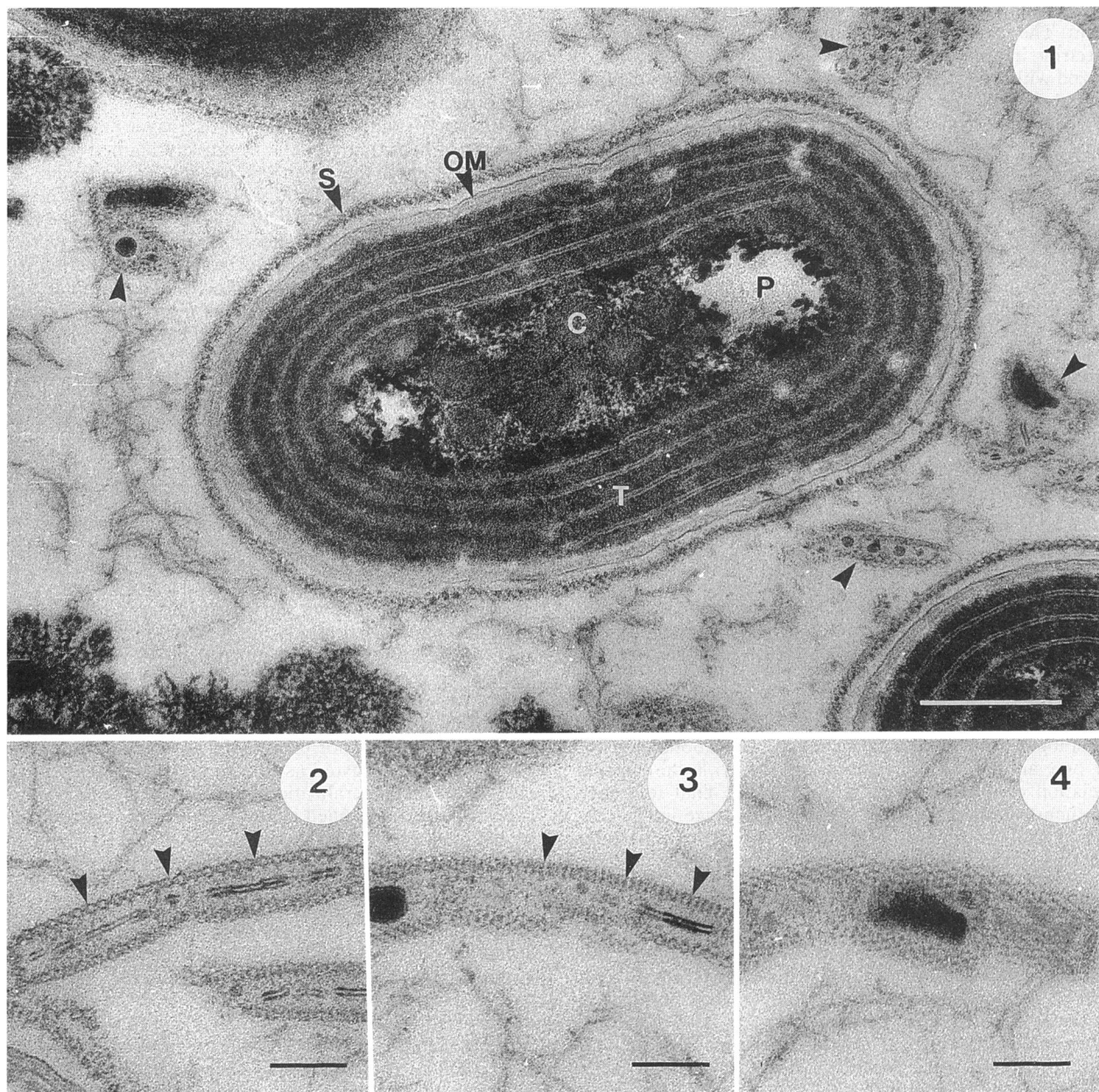
FIG. 1. Longitudinal thin section of a conventionally prepared *Synechococcus* strain GL24 cell showing some of the general features of this bacterium. The S layer (S) completely encircles the cell. Numerous S-layer fragments with associated outer membrane material can be seen surrounding the cell (arrowheads). OM, outer membrane; T, thylakoid (photosynthetic membrane); C, carboxysome; P, polyphosphate granule (all but the peripheral material was extracted during the embedding procedure). Bar = 500 nm.

FIG. 2. Detail of a conventionally prepared S-layer fragment showing the diamond pattern (arrowheads) seen when a cut is made parallel to a line of symmetry. Bar = 100 nm.

FIG. 3. An S-layer fragment, prepared as for Fig. 2, showing the pattern of parallel lines (arrowheads) resulting from a cut made perpendicular to a line of symmetry. Bar = 100 nm.

FIG. 4. When a fragment is cut tangentially, a pattern of hexagonally arranged dots, possibly corresponding to the tips (top or bottom) of the diamonds shown in Fig. 2, is often seen. Bar = 100 nm.

The information gained from computer-enhanced images also allowed a model of the approximate shape and arrangement of the individual subunits to be made (Fig. 16). This assured us that it was possible for the S-layer pattern of *Synechococcus* strain GL24 to be made up of many copies of a single molecule arranged in a particular pattern, which fits well with accepted ideas about S-layer structure (15).

To establish the precise location of initial gypsum nucleation, whole mounts of cells in early stages of mineralization (7 days) were examined. Images of fragments similar to the one shown in Fig. 9 were subjected to computer processing. Subtle changes to the ring structure and to the large, diamond-shaped pores were seen as mineralization progressed (Fig. 17 to 20). The central pore became obscured as
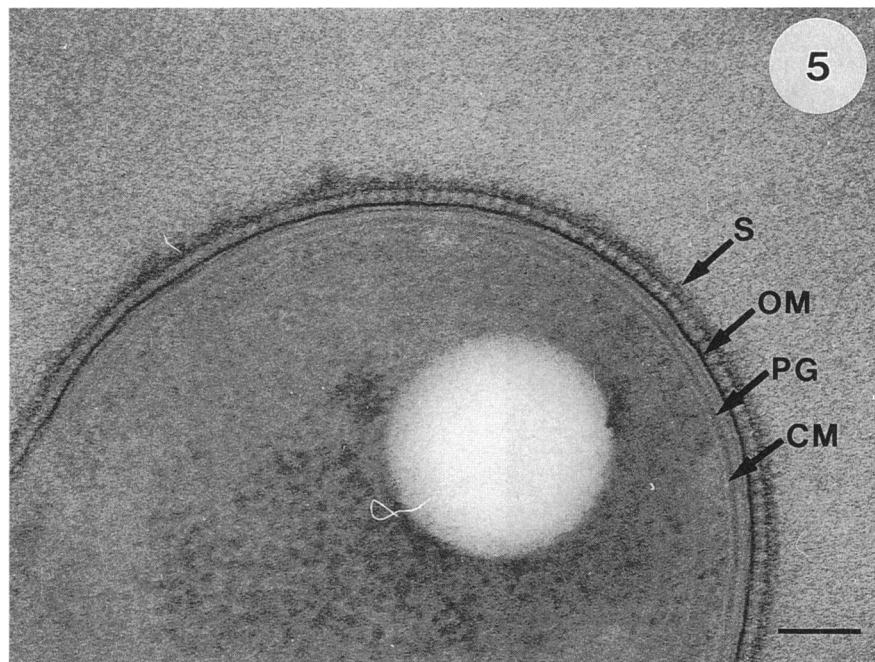
FIG. 5. Thin section of a freeze-substituted *Synechococcus* cell showing details of the envelope layers. Note that the S layer (S) seems to be joined by stems to the underlying structures. OM, outer membrane (the outer leaflet has been more darkly stained than the inner leaflet); PG, peptidoglycan; CM, cytoplasmic membrane. Bar = 100 nm.

the ring became encrusted by dense material (i.e., gypsum), while the larger pores seemed to change in shape and become encrusted around their edges, gradually becoming filled in. As the degree of mineralization increased, it became difficult to distinguish the centers of sixfold symmetry from the Y linkers in the mineralized S-layer pattern (Fig. 20). The structure of the entire morphological unit also appeared blurred because of an inherent loss of visual periodicity as the irregularly shaped mineral grains were formed. It is important to realize that the apparent decreases in pore size
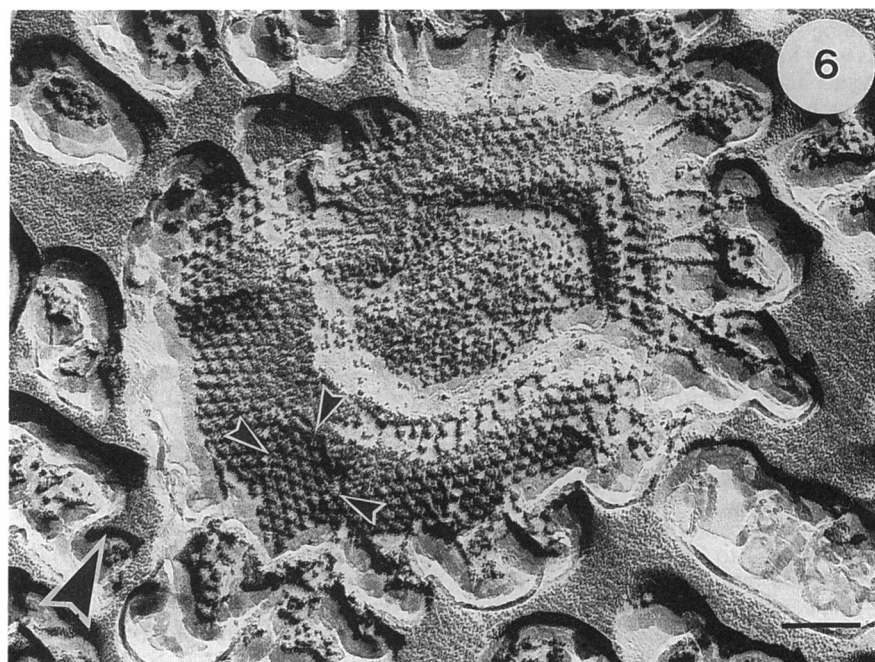

FIG. 6. Freeze fractured and -etched cell in which one pole has been exposed. A discontinuity in the S-layer lattice structure is visible (arrowheads). The large arrowhead indicates the shadowing direction. Bar = 200 nm.
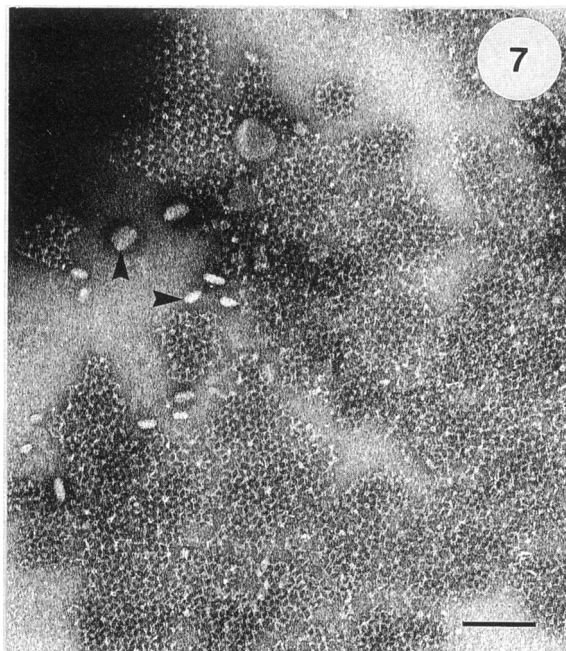
FIG. 7. Negatively stained cell showing the characteristic appearance of cells after heat treatment to release S-layer material. The cell occupies the upper lefthand corner of the micrograph. Note that the array comes off as fragments rather than as large sheets and that it is accompanied by outer membrane material (arrowheads). Bar = 200 nm.

and shape definition are actually artifacts induced by the growing gypsum crystals as they become irregularly apposed to the S-layer symmetry.

SDS-PAGE. Samples of S-layer material showed double bands in gels at M_rs of 104,000 and 109,000 (Fig. 21). No other protein bands were revealed by Coomassie blue staining, although silver staining revealed the presence of a few, very faint protein bands with lower molecular weights and an abundance of lipopolysaccharide derived from the outer membrane material which invariably accompanied the S-layer protein in all preparations.

DISCUSSION

Computer-processed images of unmineralized S layer show a delicate pattern reminiscent of that seen in unprocessed negatively stained images but with greater detail, allowing the approximate shape and arrangement of the constituent protein monomers to be seen. The morphological unit of the S layer, made up of six subunits, resembles a pinwheel. Since the main mass of the protein is in the region of the central ring, which is a center of sixfold symmetry, and the centers of the Y linkers are foci of threefold symmetry, it is an M_6C_3 S layer, according to Saxton and Baumeister (18) by their classification scheme for S-layer crystal symmetries. The *Synechococcus* strain GL24 S layer bears a superficial resemblance to the hexagonal layers present on some other bacteria (e.g., *Thermoproteus tenax* and *T. neutrophilus* [14], *Synechocystis* strain CLII [11], and the outer "punctate" layer of *Lampropedia hyalina* [2]) when low-resolution, negatively stained images are compared. However, subtle differences emerge after computer enhancement, e.g., different symmetries (*T. tenax* and *T.*

neutrophilus [14]), delta linkers (rather than Y linkers) between centers of sixfold symmetry (*Synechocystis* strain CLII [11]), and differences in morphology at the centers of sixfold symmetry (those of *T. tenax* and *T. neutrophilus* resemble stars, while those of *Synechocystis* strain CLII appear as lobed hexagons rather than the rings seen with *Synechococcus* strain GL24). Differences in the shapes of the pores outlined by the linkers also exist.

Ultrastructural studies can also give clues to the chemical nature of the S-layer protein. Biological structures are made visible in the electron microscope by staining with heavy-metal salts to increase contrast. For negative staining, we rely on the pooling of the stains in depressions of the structures to reveal their morphology. However, a certain amount of positive staining occurs also, through the interaction of the charged groups on the structure with the metal cations in the stain. For this reason, morphological and size information obtained from negatively stained material must be considered approximate rather than absolute (1). When viewing thin sections, it is precisely this positive staining effect that we rely on to visualize the structure. The different patterns seen with different orientations of the S layer on *Synechococcus* strain GL24 cells is a reflection of the presence of functional groups that are capable of binding the cationic heavy-metal stains. The appearance of diamonds (Fig. 2) likely results from the presence of negatively charged external groups on the constituent amino acids of the protein, while nonpolar amino acids are internalized, giving rise to a central nonstaining region when a cut is made through a protein mass. This binding of stains to external residues on the protein continues to be reflected when different orientations to the plane of the cut are seen as different staining patterns in the protein layer (Fig. 3 and 4). The patterns seen in thin sections do not appear to represent superpositions due to the thickness of the sections, since the spacing between adjacent periodic elements (e.g., the tips of diamonds) is the same as the center-to-center spacing (22 nm) seen in negatively stained or freeze-etched S-layer images.

The concept of external charged residues appears contrary to the observation that S-layer proteins frequently expose hydrophobic or uncharged surfaces to the external milieu (15). We have frequently observed that, in certain cases, the *Synechococcus* strain GL24 S layer does not show up at all in stained thin sections, and we have not been able to determine why it exhibits this inconsistent staining behavior. When the layer is stained, it stains intensely, indicating that there is great potential for heavy-metal binding when conditions are right. In an attempt to learn how to obtain consistently well-stained S layers in thin sections, we have tried many different treatments; cells pretreated with calcium allow visualization of the S layer upon subsequent staining with uranium and lead, although the contrast is still faint (20). It is possible that Ca^{2+} has just the proper hydrated ionic radius and charge character needed to interact with the protein and reorient its folding so that more polar residues become available for uranyl and lead ion binding.

Fragments of S layer that have been subjected to PAGE show that the S-layer protein appears as a double band. This may be due to several reasons: (i) the S layer is made up of two different proteins, (ii) the lower band represents a degradation product, (iii) the two bands represent mature and immature forms of the same protein, (iv) a proportion of the protomers in the S layer are glycosylated, or (v) a particular size of lipopolysaccharide molecule forms a tight and preferential association with the S-layer protein. Of the
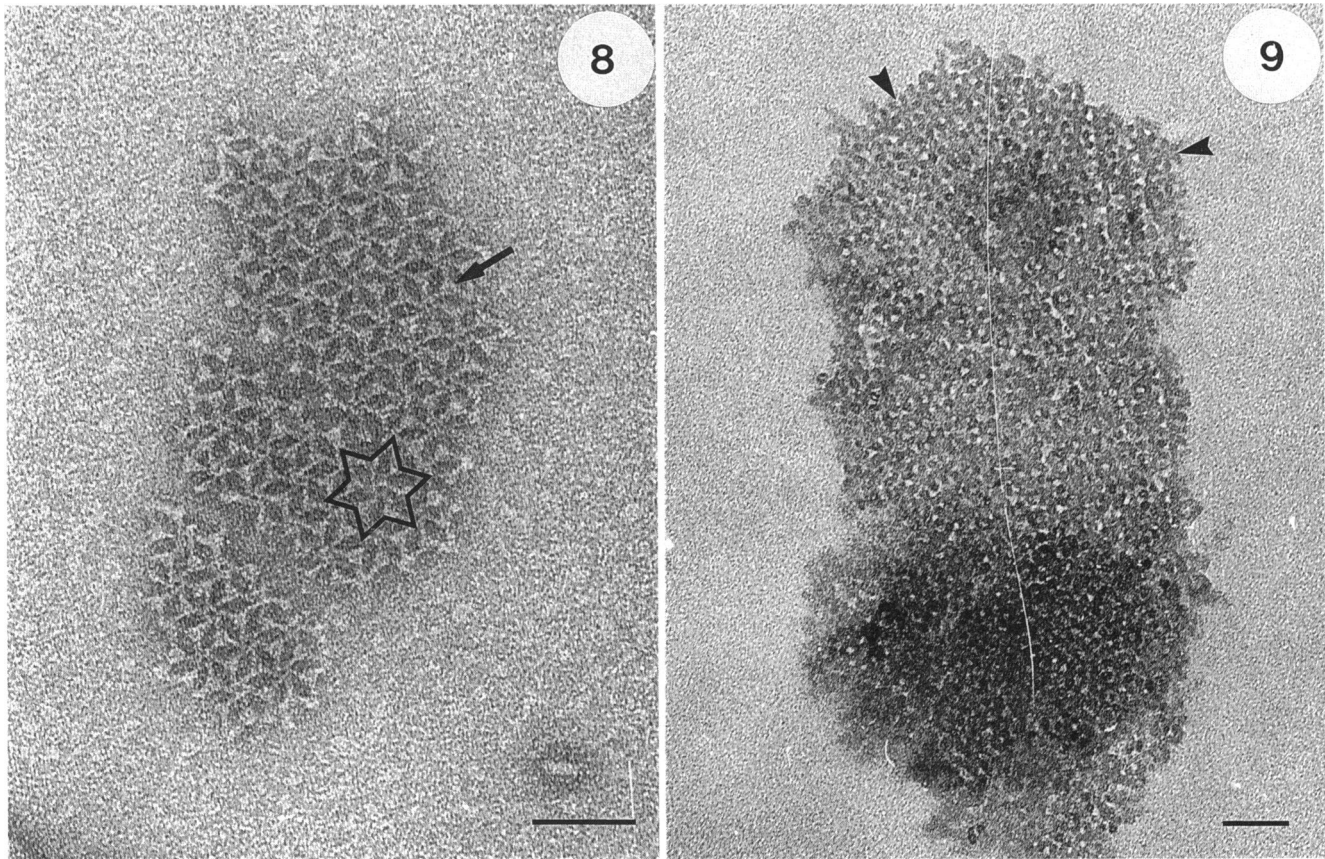
FIG. 8. Detail of a negatively stained S-layer fragment showing the symmetrical structure of the array. A hexagonally symmetrical morphological unit (pinwheel) is outlined. The arrow points to a center of threefold symmetry (Y linker). Bar = 50 nm.

FIG. 9. An unstained whole mount of a mineralized S-layer fragment in which the only contrast comes from the gypsum crystals present. Note the similarity between the elements indicated by arrowheads and the pinwheels of Fig. 8. Bar = 50 nm.

above possibilities, the last two seem the most likely explanations. A very tight association between the S layer and the underlying outer membrane has been demonstrated through rigorous attempts to selectively extract S-layer protein from the cell surface (20). Samples which contain S-layer protein always contain lipopolysaccharide, making it impossible to verify whether the monomer is a glycoprotein. Furthermore, the S layer does not appear to be made up of two different proteins on the basis of evidence from electron microscopy and computer-enhanced imaging, although these methods cannot be viewed as able to unequivocally verify this fact. The second band does not appear to be a degradation product, since it always has the same staining intensity in gels (by visual assessment only) in relation to the upper band, which also seems to go against the idea of immature proteins, rather than mature proteins, being responsible for the banding pattern.

The most remarkable feature of unstained whole mounts of *Synechococcus* strain GL24 cells grown in real and simulated lake water is that they clearly show that the S layer becomes outlined in gypsum ($CaSO_4 \cdot H_2O$). In order for mineralization to occur, Ca^{2+} is thought to bind first, and it should be an essential ingredient for the whole process. This was substantiated by the fact that the other divalent cations tested (Mg, Ba, and Sr) did not allow the S-layer pattern to be revealed. Yet, chemical studies undertaken in attempts to isolate the S-layer protein from whole cells

indicated that calcium is not important for the stability or binding of the S layer to the cell. When cells were treated with EGTA [ethylene glycol-bis(β-aminoethyl ether)-N,N,N',N'-tetraacetic acid], a specific chelator of Ca, the S-layer pattern remained intact even after prolonged (4-h) treatment (20).

As indicated earlier to explain the positive staining of thin sections, the binding of calcium to the S layer in seeming preference to other cations may result from the fact that hydrated calcium ions have just the right size (most importantly) and charge character to meld with appropriate sites within the protein fabric. It has been suggested previously that S layers, rather than being inert barriers, are dynamic structures that are capable of acting as ion exchangers and can provide ion buffering for the cell (3). The ability of the S layer of *Synechococcus* strain GL24 to mediate mineral formation may be a consequence of its ability to bind and release many different ions, regulating their concentrations in the vicinity of the cells. Because of the great abundance of Ca^{2+} and SO_4^{2-} in the lake, the formation of gypsum on cell surfaces (followed by calcite as pH rises) may be an inevitable consequence for organisms living in the lake. The S layer intercedes between the external milieu and the underlying outer membrane. In this sense, the S layer may have a protective function, allowing the cell to rid itself of minerals by shedding S-layer material when the burden becomes too great. Thus, the S layer allows the cell to control where
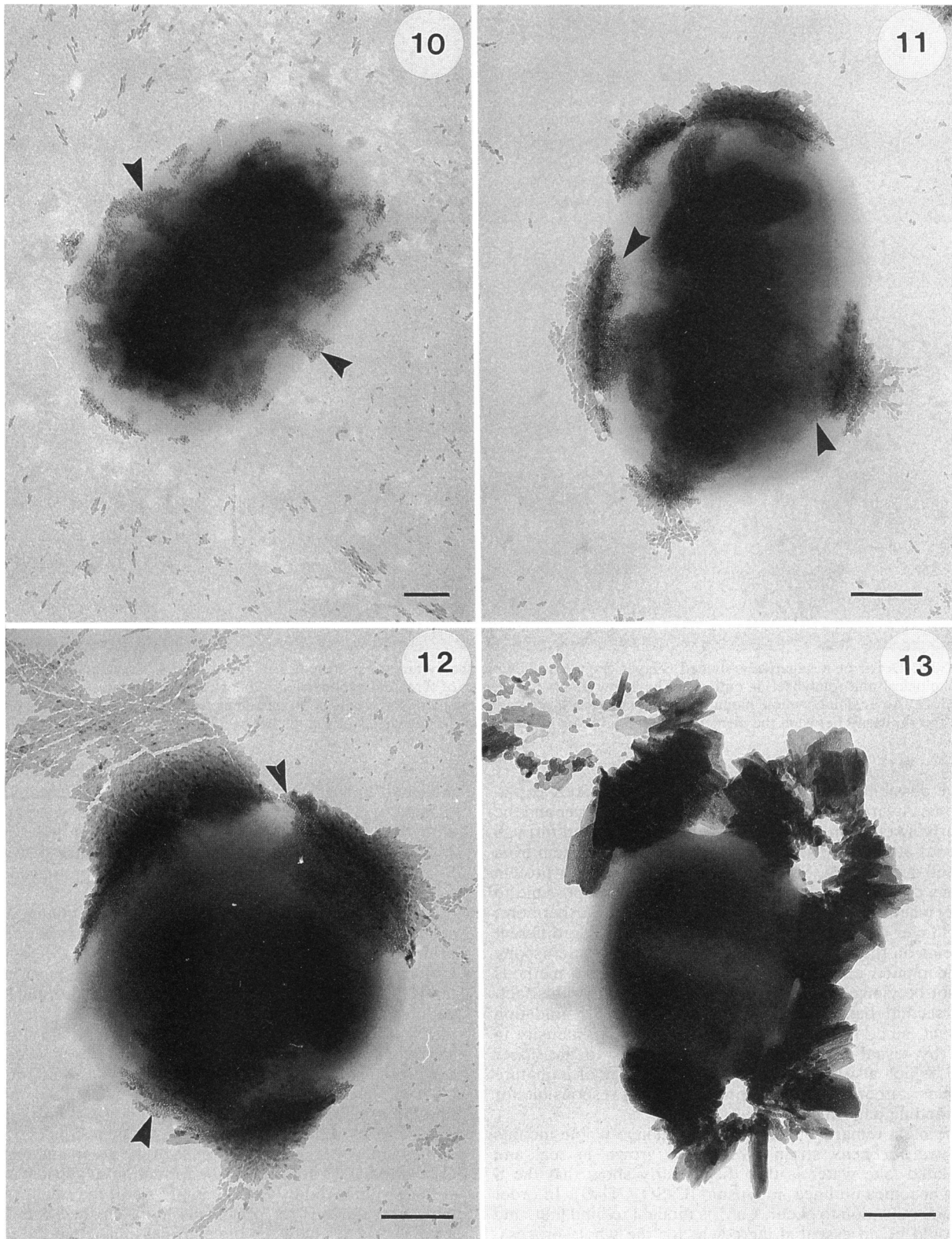
FIG. 10–13. A series of micrographs showing unstained *Synechococcus* cells at various, successive, early stages in the mineralization process. In all cases, the mineral present is gypsum. The S-layer pattern (arrowheads) gradually becomes obscured until, eventually (Fig. 13), it is no longer visible. Bars = 300 nm.
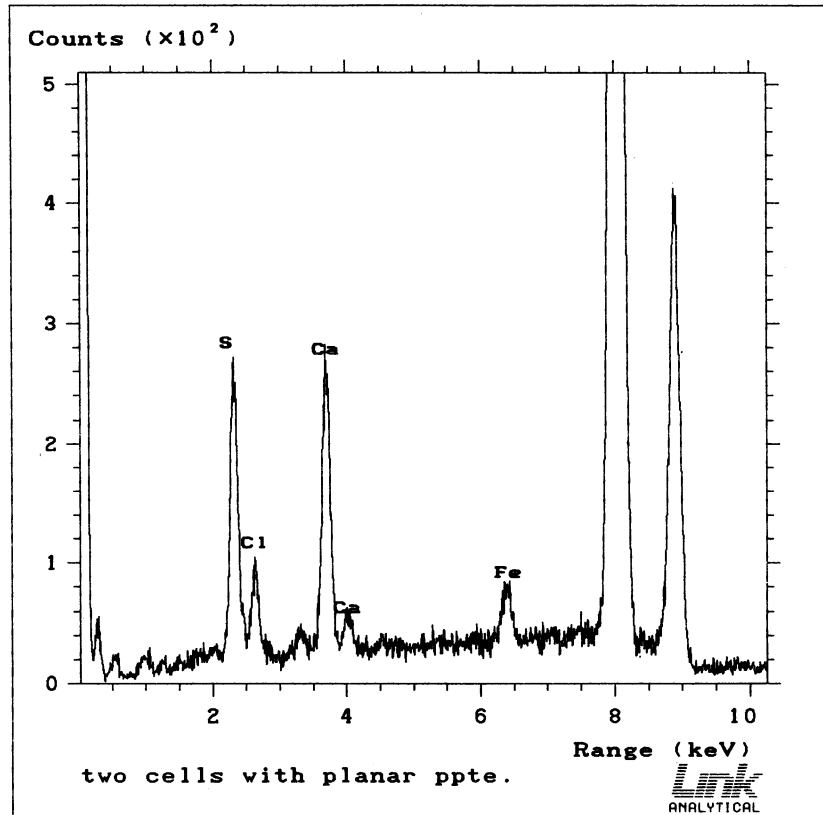
FIG. 14. EDS spectrum of a crystal similar to crystals shown in Fig. 13. Ca and S clearly predominate in the structure of these crystals. The identity of the mineral was verified by selective-area electron diffraction.

mineralization will occur and prevents the encrusting minerals from interfering with vital cell processes such as growth and division, nutrient transport, and even photosynthesis. This postulate is supported by the fact that *Synechococcus* cells growing in culture tend to shed quantities of their S layer with accompanying outer membrane material into the culture medium. One would expect that for those bacteria with S layers in natural environments where biomineralization processes occur, this shedding must be a common phenomenon. The production of S-layer protein is an ener-

gy-demanding process, and shedding of this material would seem to be a great drain on the resources of the cell. Yet, for *Synechococcus* cells, which gain their energy from light, there is little limitation to their source of energy, and perhaps the renewal of S-layer material may not be as formidable an undertaking as for cells which rely on a more limited source of energy (such as complex organic carbon), especially when the impetus for shedding (encrustation by minerals) is a powerful one. In this context, the release of S-layer material is not a wasteful activity but a necessary one.
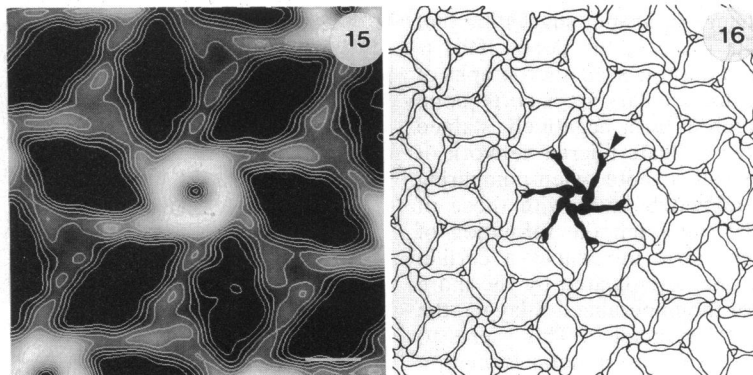

FIG. 15. Contoured, computer-processed image of a pinwheel, emphasizing pore and subunit morphologies. Bar = 5 nm.

FIG. 16. Two-dimensional model of the *Synechococcus* strain GL24 S layer showing the approximate shape and arrangement of the protomers. A single morphological unit, or hexamer, is shown in black and is a center of sixfold symmetry. A center of threefold symmetry, or Y linker, is indicated by the arrowhead.
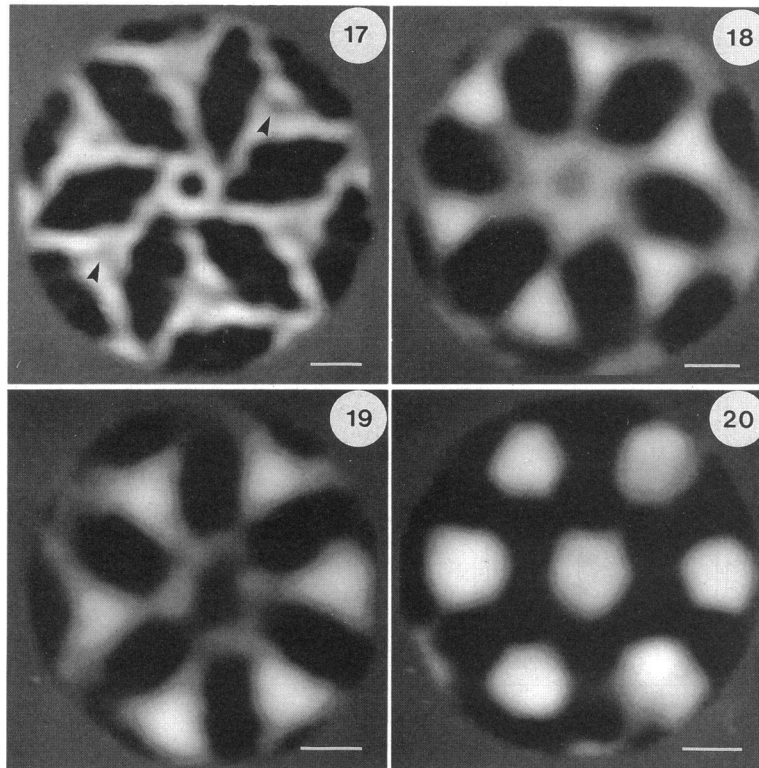
FIG. 17. Computer-processed image of the hexagonally symmetrical morphological unit (hexamer, or pinwheel) of a negatively stained, unmineralized S-layer fragment similar to the one shown in Fig. 8. The hexamer has a counterclockwise rotational orientation and possesses two types of pores: large, diamond-shaped pores and a small, circular pore in the middle of the central ring. Delineations between molecules can be seen in the Y-linker regions (arrowheads). Bar = 5 nm.

FIG. 18–20. Computer-processed images of hexamers from unstained, mineralized S-layer fragments at progressively more advanced stages in the mineralization process. Dark areas are sites of mineral formation. Note the changes in the shapes of the larger pores and the encrustation of the central ring in Fig. 18 and 19 compared with these elements in Fig. 18. Figure 20 shows a hexamer at an advanced state of mineralization in which it has become impossible to distinguish between hexamers and Y linkers, but hexagonal symmetry is still apparent. Bars = 5 nm.

This study is the first time that the initial stages of biomineralization have been detected by computer image enhancement on an S layer, and it is remarkable (though not unexpected) that it occurs on discrete periodic sites within the S layer. When images of an unmineralized, negatively stained S layer are compared with those of mineralized fragments, certain features of the mineralization process are revealed. As mineralization progresses, the diamond-shaped pores become smaller and change in shape, suggesting that the initial binding events take place in the pores. This is substantiated when one looks at unprocessed micrographs of mineralized S layer and notes that the dark areas correspond to positions of the pores, much as in a negatively stained sample, rather than outline the delicate filigree network of the protein itself. Another aspect to note when comparing processed images of a mineralized S layer with those of unmineralized samples is that, although the formation of mineral grains in the S-layer fabric introduces a certain degree of aperiodicity in the image (indicated by the more blurred computerized image of the mineralized S layer), the image retains its overall general symmetry. This seems to show that the initial binding events and mineral formation take place in an orderly fashion at sites that are regularly placed because of the intrinsic symmetry of the S layer itself.

We can now envision how sediment and bioherm formation proceed in Fayetteville Green Lake. As daylight, tem-
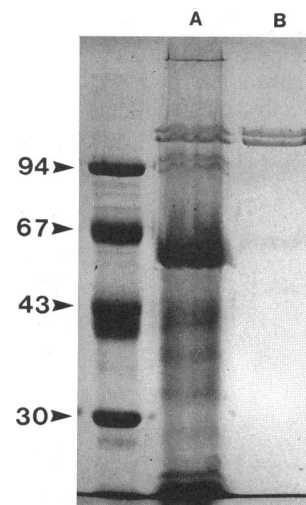
FIG. 21. SDS–12.5% PAGE gel stained with Coomassie blue to show the location of the S-layer protein. Lanes: A, profile of whole-cell protein; B, protein present in a typical S-layer preparation used in our work. The far left lane contains low-molecular-weight markers for scale. The actual molecular weights for the S-layer protein bands were calculated from a gel which included high-molecular-weight markers.

perature, and photosynthesis increase, *Synechococcus* blooms, and each cell surrounds itself with an alkaline microenvironment which alters the mineralization from gypsum to calcite. Accordingly, each cell in the increased population acts as a small nucleation granule for the growth and development of fine-grain calcite. Consequently, those cells which are planktonic contribute to a light but constant rain of mineral to the sediments, determining their marl character, while those that are benthic and adhere to the solid substratum become entombed and, over time, contribute to calcitic bioherms. For each mineral (gypsum or calcite), an energy barrier must first be overcome, and environmental factors, such as pH, contribute to the energy threshold. Accordingly, the crucial thermodynamic factor for determining a mineral phase is the initial nucleation event; once this has occurred, the preordained mineral will continue to preferentially grow. For this reason, not only intact photosynthesizing cells will mediate calcite development but also their shed S-layer fragments. Total cell numbers within a natural system may underestimate the actual biomineralization effect.

We are presently engaged in detailed analyses of the surface chemistry of *Synechococcus* strain GL24 and in a more precise assessment of this organism's ability to bind cations and anions in an attempt to further our understanding of the involvement of this cyanobacterium in mineral formation.

REFERENCES

1. **Amos, L. A.** 1974. Image analysis of macromolecular structures. J. Microsc. **100:**143–152.
2. **Austin, J. W., A. Engel, R. G. E. Murray, and U. Aebi.** 1989. Structural analysis of the S layer of *Lampropedia hyalina*. J. Ultrastruct. Res. **102:**255–264.
3. **Beveridge, T. J.** 1979. Surface arrays on the wall of *Sporosarcina ureae*. J. Bacteriol. **137:**1039–1048.
4. **Brunskill, G. J., and S. D. Ludlam.** 1969. Fayetteville Green Lake, New York I: physical and chemical limnology. Limnol. Oceanogr. **14:**817–829.
5. **Castenholz, R. W.** 1988. Culturing methods for cyanobacteria. Methods Enzymol. **167:**68–93.
6. **Graham, L. L., and T. J. Beveridge.** 1990. Evaluation of freeze-substitution and conventional embedding protocols for routine electron microscopic processing of eubacteria. J. Bacteriol. **172:**2141–2149.
7. **Harauz, G., and E. Boekema.** 1991. Processing and analysis of electron images of biological macromolecules, p. 195–218. *In* D. Hader (ed.), Image analysis in biology. CRC Press, Inc., Boca Raton, Fla.
8. **Harauz, G., E. Boekema, and M. van Heel.** 1988. Statistical image analysis of electron micrographs of ribosomal subunits. Methods Enzymol. **164:**35–49.
9. **Hitchcock, P. J., and T. M. Brown.** 1983. Morphological heterogeneity among *Salmonella* lipopolysaccharide chemotypes in silver-stained polyacrylamide gels. J. Bacteriol. **154:**269–277.
10. **Jensen, T. E., and L. M. Sicko.** 1972. The fine structure of the cell wall of *Gloeocapsa alpicola*, a blue-green alga. Cytobiologie **6:**439–446.
11. **Karlsson, B., T. Vaara, K. Lounatmaa, and H. Gyllenberg.** 1983. Three-dimensional structure of the regularly constructed surface layer from *Synechocystis* sp. strain CLII. J. Bacteriol. **156:**1338–1343.
12. **Laemmli, U. K.** 1970. Cleavage of structural proteins during the assembly of the head of bacteriophage T4. Nature (London) **227:**680–685.
13. **Lounatmaa, K., T. Vaara, K. Österlund, and M. Vaara.** 1980. Ultrastructure of the cell wall of a *Synechocystis* strain. Can. J. Microbiol. **26:**204–208.
14. **Messner, P., D. Pum, M. Sára, K. O. Stetter, and U. B. Sleytr.** 1986. Ultrastructure of the cell envelope of the archaebacteria *Thermoproteus tenax* and *Thermoproteus neutrophilus*. J. Bacteriol. **166:**1046–1054.
15. **Messner, P., and U. B. Sleytr.** 1992. Crystalline bacterial cell-surface layers, p. 213–275. *In* A. H. Rose and D. W. Tempest (ed.), Advances in microbial physiology, vol. 33. Academic Press, London.
16. **Morrisey, J. H.** 1981. Silver stain for proteins in polyacrylamide gels: a modified procedure with enhanced uniform sensitivity. Anal. Biochem. **117:**307–310.
17. **Saxton, W. O., and W. Baumeister.** 1982. The correlation averaging of a regularly arranged bacterial protein. J. Microsc. **127:**127–138.
18. **Saxton, W. O., and W. Baumeister.** 1986. Appendix: principles of organization in S layers. J. Mol. Biol. **187:**251–253.
19. **Schultze-Lam, S., G. Harauz, and T. J. Beveridge.** 1992. Characterization of the S layer from the cyanobacterium *Synechococcus* GL24, abstr. J-2, p. 253. Abstr. 92nd Gen. Meet. Am. Soc. Microbiol. 1992. American Society for Microbiology, Washington, D.C.
20. **Schultze-Lam, S.** Unpublished data.
21. **Thompson, J. B., and F. G. Ferris.** 1990. Cyanobacterial precipitation of gypsum, calcite, and magnesite from natural alkaline lake water. Geology **18:**995–998.
22. **Thompson, J. B., F. G. Ferris, and D. A. Smith.** 1990. Geomicrobiology and sedimentology of the mixolimnion and chemocline in Fayetteville Green Lake, New York. Palaios **5:**52–75.
23. **van Heel, M., and W. Keegstra.** 1981. IMAGIC: a fast, flexible and friendly image analysis software system. Ultramicroscopy **7:**113–130.